NONLINEAR TIME-DOMAIN STRUCTURE/AERODYNAMICS COUPLING IN SYSTEMS WITH CONCENTRATED STRUCTURAL NONLINEARITIES

Félix Arévalo, Pablo García-Fogeda, Héctor Climent
AIRBUS Military, Structural Dynamics and Aeroelasticity Department
ETSIA, Universidad Politécnica de Madrid

Keywords: *Aeroelasticity, Nonlinear, Missile, Freeplay, Hysteresis*

Abstract

This paper details a practical approach for predicting the aeroelastic response (structure/aerodynamics coupling) of flexible pod/missile-type configurations with freeplay/hysteresis concentrated structural nonlinearities. The nonlinear aeroelastic response of systems in the presence of these nonlinearities has been previously studied by different authors; this paper compiles methodologies and related airworthiness regulations. The aeroelastic equations of the pod/missile configuration are formulated in state-space form and time-domain integrated with Fortran/Matlab codes developed ad hoc for dealing with freeplay/hysteresis nonlinearities. Results show that structural nonlinearities change the classical aeroelastic behaviour with appearence of non-damped motion (LCOs and chaotic motion).

1 Introduction

This report analyses the time-domain aeroelastic response of flexible slender wing+body configurations in the presence of freeplay/hysteresis concentrated structural nonlinearities. The theoretical formulation and methodology are directly applicable for the preliminary design of pod/missile-type configurations, characterizing the nonlinear aeroelastic response on the entire flight envelope and predicting the effect of the structural nonlinearities on stress or fatigue. In addition, the solving procedure of the time-domain aeroelastic equations is based on a methodology and tools that can be extended for using with complex aircraft-type configurations.
The first part of the paper is devoted to review the state of the art of the analysis of structural nonlinearities from the aeroelastic standpoint. Both technical publications and civil/military airworthiness regulations are reviewed, discussing the current methodologies and analyzing advantages and disadvantages of each one.
The following sections will describe the aeroelastic model of a flexible missile configuration. The structural model is a beam-like flexible finite element model for the missile body while the all-movable control surfaces are assumed to behave as rigid plates. The inertia is based on a mass per unit length distribution along the longitudinal axis of the missile, and the aerodynamics is calculated with the unsteady slender body theory. The structural nonlinearities are located at the missile-to-pylon fittings or at the all-movable control surfaces rotation due to freeplay/hysteresis of the actuators or even wear of the hinge bearings.
The aeroelastic equations are formulated into the state-space form and are time-domain integrated with Fortran/Matlab codes developed ad hoc for treating these kind of piecewise linear nonlinearities. The report details particular features on the state-space formulation, time integration, and post-processing of the system response, that are

shown to be useful not only for pod/missile-type configurations but also for more complex systems (aircraft-type) when dealing with concentrated nonlinearities.
The test case to show the previous methodology and tools is a conventional missile-type configuration. Two possible boundary conditions (missile hanged on the aircraft or free-flying) are combined with different location (missile-to-pylon fittings or control surface rotation) of a freeplay or hysteresis nonlinearity. In addition, parametric variations on the nonlinearity characteristics are studied: deadband amplitude, deadband center, preload, and initial boundary conditions.

2 Regulations & State of the Art

Different Civil and Military Airworthiness Regulations contain paragraphs regulating procedures and techniques for predicting and/or preventing the effects of local structural nonlinearities. As example of typical requirements, table 1 below shows the acceptable freeplay limits according to military specification MIL-A-8870C.

CONTROL SURFACE	FREEPLAY [deg]	
Trailing Edge Control Surface	Extends outboard of 75% main surface span	0.13
	Extends outboard to between 50% and 75% main surface span	0.57
	Extends outboard to less than 50% main surface span	1.15
Tab	Tab span $\geq$ 35% control surface span	0.57
	Tab span $<$ 35% control surface span	1.15
All-movable Control Surface	0.034	

Table 1 Control Surface Freeplay according to MIL Specification.

Table 2 summarises the main methodologies and calculation methods that are currently applied when dealing with local structural nonlinearities.

3 Time-Domain Integration: A Practical Approach

Different authors have shown that local *piecewise-linear* nonlinearities cause chaotic-type complex responses, and the unique methodology that is able to predict chaotic behaviour is the nonlinear time-domain approach. This paper follows this methodology, the aeroelastic equations are written in state-space form and integrated with Fortran 90 codes developed ad hoc for treating *freeplay/hysteresis* nonlinearities. This section describes the main characteristics of these codes.
The experience on the missile configuration of this paper ([4]) and also on other industrial projects inside Airbus Military ([3]) has led to incorporate the following features into the integration codes:

1. **Capturing of the corner points** of the freeplay/hysteresis nonlinearity. During the time-domain integration process, the aeroelastic equations must switch once the system crosses any corner of the nonlinearity. If the system does not switch at the exact corner point, integration errors will acumulate and the solution could diverge. This paper uses the *Illinois* method (Figure 1b) for locating the exact corner points. Figure 1a compares the *Illinois* method (time step 0.001 [sec]) with classical Runge-Kutta integrations without detection of switching points. The *Illinois* method converges with time step 0.001 [sec], while Runge-Kutta solutions should use time-step of 10^{-5} [sec] to supply the same accuracy as *Illinois*.

2. **Real-time response detectors**. The aeroelastic characterization of the flight envelope of an aircraft could lead to thousands of time-domain integrations, varying flight speed, altitude, and parameters of the nonlinearity. It is interesting to include into the code a *detector* that identifies as soon as possible the type of motion (damped, LCO, or flutter), writes out the necessary information (response type, frequency, and amplitude), and continues inmediately with the following integration point. This procedure is critical to avoid wasting time integrating damped responses or clearly iden-

METHOD	DEFINITION	ADVANTAGES	DISADVANTAGES
Time-Domain Integration of the Aeroelastic Equations	The aeroelastic equations are written in the state-space form (time-domain 1st-order differential equation) and time-integrated with a suitable integration scheme. The state-space approach requires to calculate the generalized aerodynamic forces in the time-domain, a calculation that is straightforward in particular problems as incompressible 2D or 3D flow ([2] and[10] respectively), quasi-steady aerodynamics ([12] y[15]) or unsteady slender body theory ([4]). However, other methods like Double-Lattice[1], used extensively in the industry, need of mathematical tools (rational approximation methods of Roger&Abel[6], Burkhart[7], Padé[18], or Karpel[14]) to transfer aerodynamic forces from frequency- to time-domain. The time-domain integration is performed by different methods: Runge-Kutta, Newmark[3], Houbolt's Finite Difference Method[17], or Henon's method[8].	-Capture all types of reponses: damped, periodic and chaotic motion. -The state-space approach allows coupling with Flight Control Laws[5].	-Time-domain integration increases computation times. -Complexity of the post-processing.
Time-marching method / Reduced Order Models ROMs.	Direct coupling between CFD (Computational Fluid Dynamics) and CSM (Computational Structural Model)[16]. Reduced Order Model ROMs are used for simplifying the aerodynamics by reducing the number of aerodynamic states.	-Capture all types of reponses: damped, periodic and chaotic motion.	-Computational cost.
Quasi-linear methods: Describing Function or HBM	System response is assumed to be harmonic, and the local nonlinear stiffness is substituted by an *equivalent linear stiffness* that results from retaining the fundamental harmonic term of the Fourier series of the nonlinearity. This method is extensively used in the industry. Reference [4] contains a detailed description of the method and different variations of it for improving its capabilities.	-Aerodynamic forces in the frequency domain. -Low computation time.	-No of high-freq responses. -No accuracy in freeplay-type nonlinerity. -No accuracy in local loads prediction.
Stability analysis in Laplace domain.	Harmonic balance method combined with classical p-K solution of the aeroelastic equations[11].	-Coupled with classical tools (freq-domain).	-No high-freq response.
Numerical Continuation Methods.	Qualitative analysis of the response by calculating of the bifurcation diagrams of the system, previously written in the state-space form.	-Low computational cost. -No freeplay-type nonlin. -No aperiodic response.	-Only qualitative results.
Point Transformation Method.	A piecewise linear system can be solved by analytical integration of linear systems with classical tools as the *transition matrix*. The state-space equations are *switched* when changing from a linear zone to another within the piecewise nonlinearity.	-Efficient computation.	-Only piecewise linear systems.
Center Manifold Method.	Apply a linear transformation on the state-space equations and solve a differential equation with the eigenvalues with zero real part[19].	-Low computational cost.	-No freeplay-type nonlin.
Normal Form Theory.	Solve state-space equations with changes of variables[19].	-Low computational cost.	-No freeplay-type nonlin.
Asymptotic Expansion Methods.	Perfome asymtotic expansion of state-space equations with the *singular perturbation method*[9].	-Low computational cost.	- U_∞ close to $U_{flutter}$. -No freeplay-type nonlin.

Table 2 Civil and Military Airworthiness Regulations with paragraphs regulating procedures for preventing the effects of local structural nonlinearities.

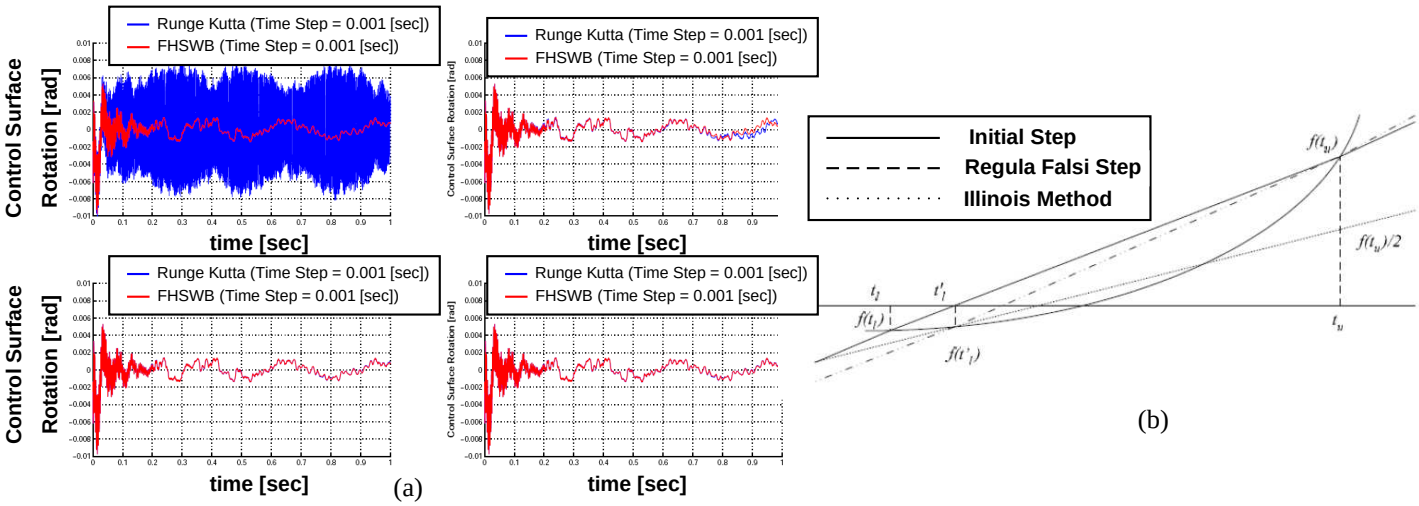

Fig. 1 (a) Comparison of the code used in this paper (time step 0.001 [sec]) with classical Runge-Kutta method with different time-steps (from 0.001 to 1.E-6 [sec]). (b) Illinois method for capturing the exact corner point of the freeplay/hysteresis nonlinearity.

tified LCOs. The following conditions are used as motion *detectors* ([4]):

- Two damped motion *detectors*: (1) Square mean of the non-dimensional generalized velocities ($\sum(d\hat{\xi}_i/d\hat{t})^2 < 10^{-4}$) (2) Distance of the system to each corner point of the nonlinearity ($< 10^{-4}$). If any of the previous conditions repeats consecutively 50 times, the code considers damped motion, stops the integration and passes to the next integration point.
- One LCO motion *detector*: The code saves packages of 50 consecutive max/min of the nonlinear DOF in vectors as $LCO_j(1:50)$ and compares these packages throughout the following equation: $LCODetector = \sum_{i=1}^{i=50}\sqrt{[LCO_j(i) - LCO_{j+1}(i)]^2}$. If the variable *LCODetector* is less than 10^{-10}, then it means that the two packages are identical and is precluding the appearance of an harmonic LCO. The code considers that an LCO has been reached if 4 consecutive identical packages occur.
- Three flutter *detectors*: (1) Absolute value of a defined-by-user output reachs a maximum value (2) Square mean of the non-dimensional generalized coordinates ($\sum\hat{\xi}_i^2 > 10^{+6}$) (3) Square mean of the non-dimensional generalized velocities ($\sum(d\hat{\xi}_i/d\hat{t})^2 > 10^{+6}$). Once one of the three conditions is reached, the code stops and goes to the next integration point.

3. Unique Modal Base **IOB**. A system with a freeplay/hysteresis nonlinearity changes the stiffness as passing through the different zones of the nonlinearity. This stiffness variation makes the system to change of normal modes (modal base) as the system crosses the corners of the freeplay/hysteresis nonlinearity. Choosing different modal bases at the two sides of a corner point could lead to discontinuities due to the inhability to transfer the boundary condition from one to the other modal base. In a modal approach, the only way of solving this problem is by using an unique modal base. For this particular problem ([4]), it is used the IOB (In/Out Base), that is composed by the modal base of the nominal system augmented with the rigid body mode obtained after dropping down to zero the stiffness of the nonlinear DoF. This modal base has been also used in

other projects as the Airbus Military Aerial Refuelling Boom System (Figure 2), obtaining satisfactory results.

Fig. 2 Boom System in AIRBUS Military A310-Demo platform

4. Modules for post-processing the system response: PSD analysis, phase-plane plots, and bifurcation diagrams.

5. Modules for characterization of the chaotic response: Poincaré maps for detecting chaos and a magnitude that is introduced, the Dispersal Rate DIRA, that quantifies the chaos intensity.

4 Application Case: Missile/Pylon Configuration

The previous methodology is applied to the missile-type configuration shown in Figure 3. Two cases are analyzed: *lateral* aeroelastic stability of a missile installed into a flying platform (missile/pylon in Figure 3a) and *longitudinal/lateral* aeroelastic stability of a free-flying missile. The missile geometry is sketched in Figure 3b and the freeplay/hysteresis nonlinearity is shown in Figure 3c.

4.1 Aeroelastic Model

4.1.1 Generalities

The time-domain aeroelastic equations are formulated by coupling the following Structural, Aerodynamic and Flight Control Laws (FCLs) models:

- Structural Model: The missile is composed of body and control surface(s) as main structural components. The body usually has a large *fineness ratio* (ratio of the body length to its maximum width) and control surfaces are low *aspect ratio* wings. The large fineness ratio makes the body mainly flexible along the longitudinal axis and an appropiate structural model is a beam-like structure. On the other hand, the low-aspect-ratio control surface behave as a rigid plate. The mass properties are defined via the following *mass-per-unit-length* functions: for the body, $m_b(x) = 25.0 + 50.0 \cdot \frac{x}{L}$ [Kg/m]; for the control surfaces, $m_w(x) = 25 \cdot (\frac{x}{L} - \frac{x_0}{L})$ [Kg/m]. L is the body length and x_0 is the x-coordinate of the control surfaces leading edge at the root station (see Figure 3b).

- Aerodynamic Model: Unsteady Slender Body Theory formulated in a body-fixed curvilinear reference system.

- Flight Control Laws (FCLs): For these analyses, classical flutter is assumed, i.e., no FCLs and the control surface response is goberned by the actuators stiffness.

4.1.2 Unsteady Aerodynamics

The unsteady generalized forces are calculated using the *Slender Body Theory* formulated in the body reference system (see Figure 4). If $w(x;t)$ is the body center line deformation, the velocity potential (assuming inviscid, adiabatic, and irrotational flow) is written as:

$$\Omega(x,y,z;t) = U_\infty \left[x + z\frac{\partial w}{\partial t}(x;t) \right] + \Phi(x,y,z;t) =$$
$$= U_\infty \left[x + z\frac{\partial w}{\partial t}(x;t) \right] + \phi_0(x,y,z) + \phi(x,y,z;t)$$

where $\phi_0(x,y,z)$ is the zero-deformation transverse velocity potential (thickness effect) and $\phi(x,y,z,t)$ is the unsteady velocity potential associated to $w(x;t)$.

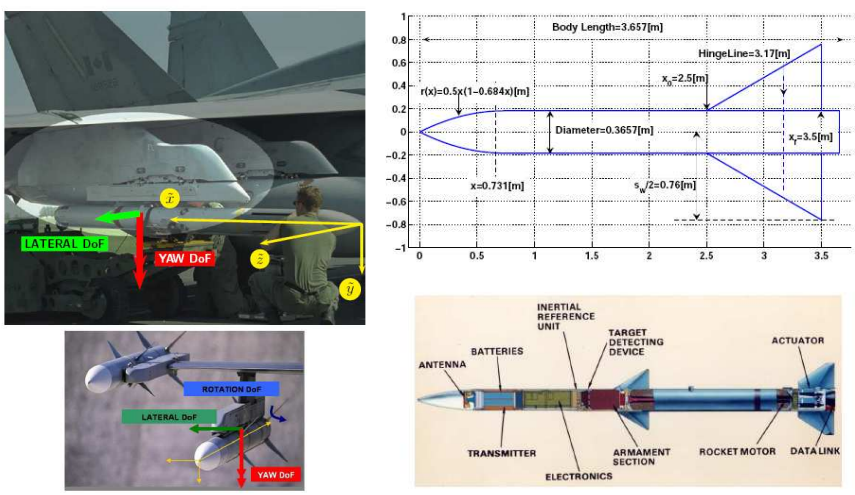

(a) (b) (c)

Fig. 3 (a) DOFs of the pod/missile-type configuration (left figure) and definition of the hysteresis nonlinearity (right figure) (b) Missile configuration analyzed into this paper (upper figure) compared with the standard AMRAAM missile (botton figure) (c) Freeplay/Hysteresis Nonlinearity

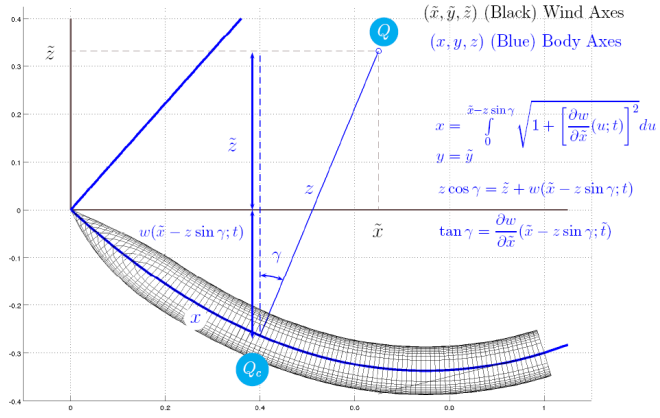

Fig. 4 Body-fixed reference system to solve the Slender Body Unsteady Aerodynamics.

Once assumed axial simmetry, the potential $\phi_0(x,y,z)$ is directly calculated by classical Slender Body Theory:

$$\phi_0(x,r;t) = U_\infty R(x)\frac{dR}{dx}(x)\ln\frac{r}{L} + g(x,M_\infty)$$

being $R(x)$ the body radius, r the radial coordinate, and L the body length used as reference magnitude. The potential $\phi(x,r,\theta;t)$ is calculated by *conformal transformations* that depends on the vertical motion $w(x;t)$ of each transverse section. The deformation is written as:

$$w(x;t) = \sum_{i=1}^{m}\psi_i(x)\xi_i(t) =$$
$$= \sum_{i=1}^{m}\psi_{i,b}(x)\xi_i(t) + \sum_{i=1}^{m}\psi_{i,wb}(x)\xi_i(t) = WjB + WrB$$

where $\psi_{i,b}(x)$ represents the i-mode contribution of the body-wing joined motion (**WjB**), while $\psi_{i,wb}(x)$ represents the i-mode contribution of the wing deformation relative to the body (**WrB**). Each contribution uses a different *conformal transformation* that are detailed in [4]. Finally, the *i-mode Generalized Aerodynamic Force* Q_i is written as a linear combination of the Generalized Coordinates ξ_i ([4]):

$$\frac{Q_i}{q_\infty L^2} = \sum_{i=1}^{m}\left[q_{\xi_i\xi_j}\hat{\xi}_j + q_{\xi_i\dot{\xi}_j}\frac{1}{\hat{U}_\infty}\frac{d\hat{\xi}_j}{d\hat{t}} + q_{\xi_i\ddot{\xi}_j}\frac{1}{\hat{U}_\infty^2}\frac{d^2\hat{\xi}_j}{d\hat{t}^2}\right]$$

4.2 Missile Configurations and Location of the Nonlinearity.

Figure 5 summarises the missile configurations that have been analyzed.

The missile/pylon configuration (**S01**) is considered rigid (**RIG**) and the nonlinearity freeplay or hysteresis is located in three possible locations: lateral motion of missile/pylon (**LAT**), yaw

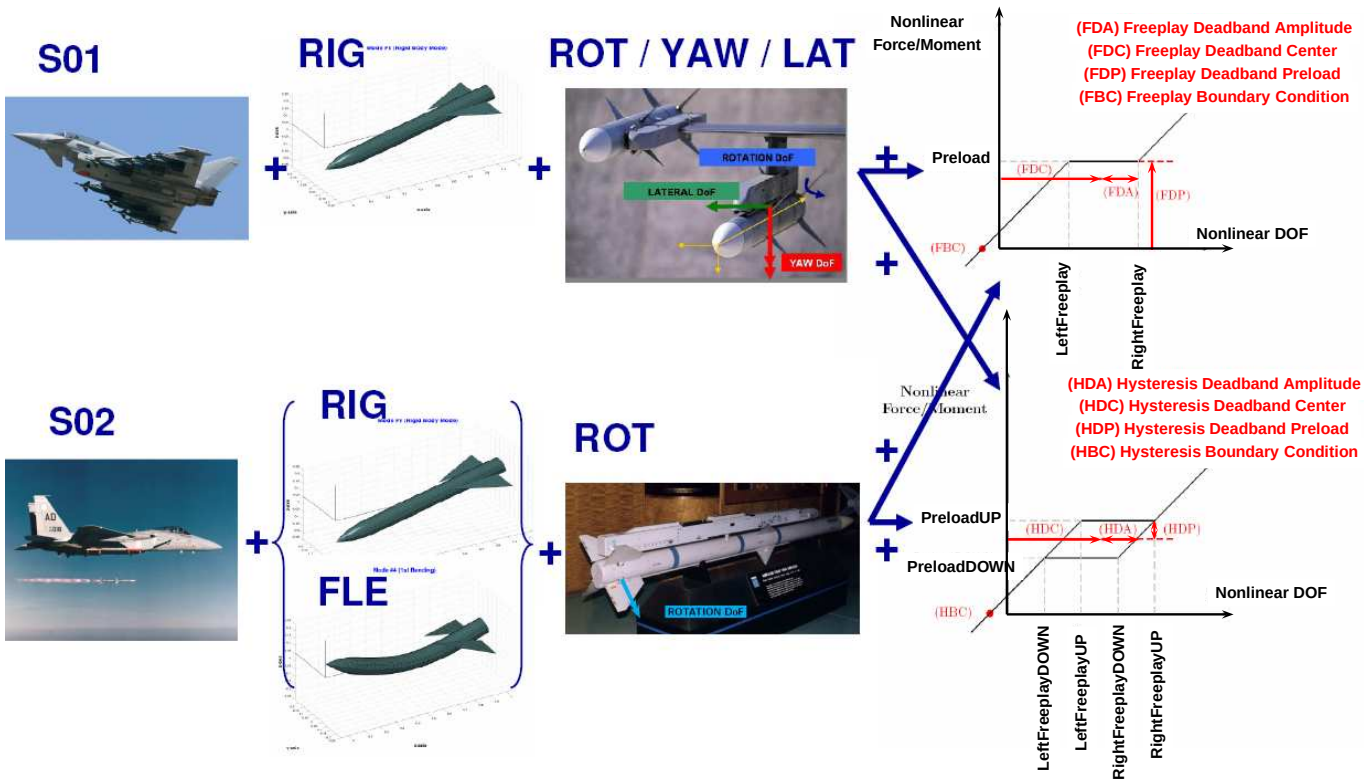

Fig. 5 Summary of missile configurations analyzed into this paper.

motion of missile/pylon (**YAW**), and control surface rotation (**ROT**).

The free-flight missile configuration (**S02**) can be rigid (**RIG**) or flexible (**FLE**) and the freeplay or hysteresis nonlinearity is located at the control surface rotation (**ROT**).

Besides this, and for each configuration, parametric variations are performed on the main characteristics of the nonlinearity: deadband amplitude (**DA**), deadband center (**DC**), deadband preload (**DP**), and initial boundary conditions (**BC**).

5 Results

5.1 Introduction

The following sections summarise the linear and nonlinear flutter analyses performed on the missile configuration. All calculations assume initial steady flight at sea level.

5.2 Linear Flutter

Before characterizing the nonlinear aeroelastic behaviour, it is necessary to analyze the *linear flutter* of the nominal stiffness and zero-stiffness configurations for understanding the main flutter mechanisms. The lowest speed flutter mechanism is a coupling of the YAW mode with the control surface rotation (ROT). Table 3 compare flutter speeds of the nominal system calculated with the codes of this paper ([4]) and MSC.NASTRAN SOL145. The Doublet-Lattice (MSC.NASTRAN) is less appropiate for calculating the interference lifting surfaces/body than the Unsteady Slender Body Theory, which imposes the zero-flow bondary condition at the exact body surface. That is the reason why including the body aerodynamics or not (AERO OFF) introduces important differences. This effect is also relevant in case of mild flutter. Table 4 details the flutter speed for zero stiffness at the relevant degrees of freedom. The zero-stiffness situation should correpond to the system while passing through the deadband zone of the

freeplay/hysteresis nonlinearity.

CONF	RIGid FLExible	BODY AERO	Flutter Speed (KTAS)		DIF[%]
			NASTRAN	FHSWB	
S01	RIG	ON	486.	496.	2.06
		OFF	484.	470.	2.98
S02	RIG	ON	562.	616.	8.77
		OFF	572.	596.	4.03
	FLE	ON	442.	241.	83.40 (*)
		OFF	196.	262.	25.19 (*)

(*) Not relevant: Mild flutter mechanism.

Table 3 MSC.NASTRAN vs [4]: Linear Flutter Speed (KTAS) of the NOMINAL system.

CONF	RIGid FLExible	Flutter Speed (KTAS)			
		nominal	$K_{ROT}=0$	$K_{LAT}=0$	$K_{YAW}=0$
S01	RIG	496.	331.	489.	381.
S02	RIG	616.	0.	N/A	N/A
	FLE	241.	0.	N/A	N/A

Table 4 MSC.NASTRAN vs [4]: Linear Flutter Speed (KTAS) of the K=0 system.

5.3 Nonlinear Aeroelastic Response

5.3.1 Missile/Pylon Configuration (S01)

The missile is assumed to be rigid (RIG) and freeplay or hysteresis nonlinearities are located at the three possible degrees of freedom: missile control surface rotation (ROT), pod/pylon yaw (YAW), and pod/pylon lateral motion (LAT). In addition, the main parameters of the nonlinearity are studied: deadband amplitude (FDA/HDA), nonlinearity center (FDC/HDC), and preload (FDP/HDP).

The following conclusions have been obtained: (1) Nonlinearities lead to LCO/Chaos below linear flutter speed (2) *Preload* tends to increase the U_{LCO} (Flight Speed of LCO appearance) (3) Nonlinearities in a mode that is not involved into the flutter mechanism (LAT mode) do not modify the linear flutter behaviour (4) Nonlinearities in the YAW mode increase the linear flutter speed (5) Hysteresis nonlinearity has more tendency to cause chaotic response than freeplay nonlinearity. The chaotic-type response will be analyze in the following section.

From the previous results, one particular case for the hysteresis nonlinearity has been selected and is shown in Figure 6.

Figure 6(a) represents the number of characteristics frequencies of the system response as a function of the KTAS Flight Speed (x-axis) and hysteresis deadband amplitude (y-axis) for an hysteresis nonlinearity located at the control surface rotation. Figure 6(b) shows a bifurcation diagram with chaotic motion (random number of points) around 250-275 KTAS.

5.3.2 Free-Flight Missile Configuration (S02)

The missile body can be rigid (RIG) or flexible (FLE), and freeplay/hysteresis nonlinearities are located at missile control surface rotation (ROT). In addition, the main parameters of the nonlinearity are studied: deadband amplitude (FDA/HDA), nonlinearity center (FDC/HDC), and preload (FDP/HDP).

Two conclusions are considered relevant: (1) For the rigid body (RIG), the *Preload* increases the Flight Speed (KTAS) of LCO appearance and (2) For the flexible body (FLE), a low-speed *mild flutter* mechanism appears (around 230 KTAS). This mild flutter is not modified by the presence of structural nonlinearities.

6 Chaotic Response: DIRA Parameter

The complex behaviour of the chaotic response can be characterized by different methods ([4]). PSD analyses, bifurcation diagrams, Poincaré maps, Lyapunov exponents, or 2D phase planes are the most commonly used tools in the literature. This paper uses the Poincaré map for a *qualitative* detection of chaos response, and introduce a novel parameter (Dispersal Rate *DIRA*) for a *quantitative* analysis of the chaos.

Figure 7 shows two Poincaré maps calculated for two different flight speeds. Each map shows pairs $(\hat{\xi}_3, d\hat{\xi}_3/d\hat{t})$ at a defined time $t = t^*$[1], where $\hat{\xi}_3$ is the normal mode associated to the nonlinearity (control surface rotation). Each pair

[1]Time $t = t^*$ should be large enough for having a stabilized chaos. Finally, the results do not depend on selected time t^*.

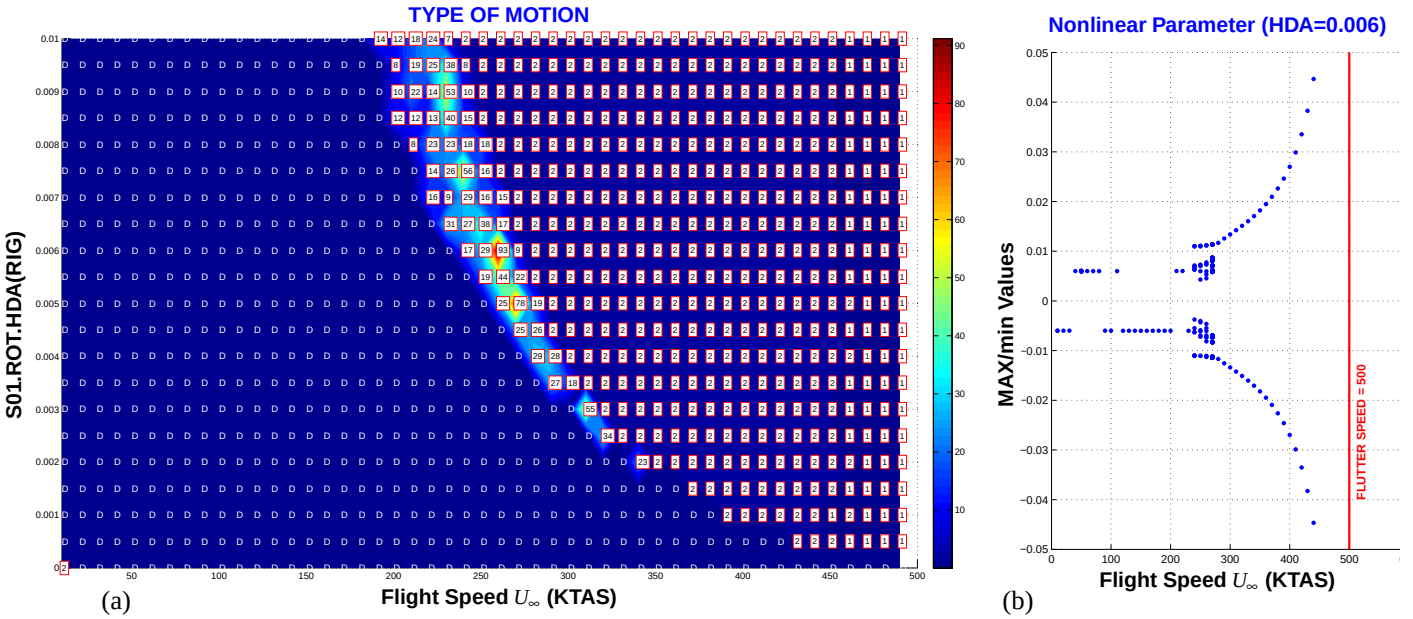

Fig. 6 (a) Analysis of the missile control surface rotation response (case RIG.S01.ROT.HDA): number of characteristic frequencies as a function of flight speed (KTAS) and hysteresis deadband amplitude (b) Bifurcation diagram (representation of max/min) for HDA=0.006.

$(\hat{\xi}_3(t^*), d\hat{\xi}_3/d\hat{t}(t^*))$ is obtained by solving the state-space equations with a initial condition close to a nominal one (difference less than 1%).

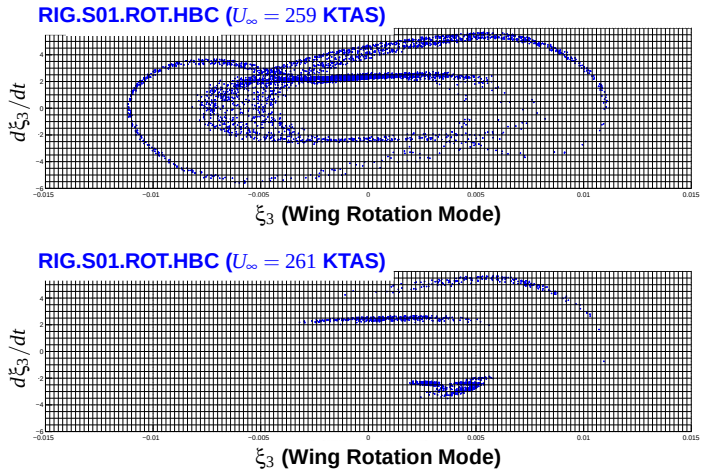

Fig. 7 Poincaré Map (Generalized Speed vs Generalized Coordinate) with the $\Re^2$ partition defined for calculating the DIRA parameter.

Based on these Poincaré maps, the following DIRA parameter is introduced for quantifying the chaos:

$$DIRA(I,P) = \frac{N - N_0}{N} \cdot 100$$

where I is an $\Re^2$ interval that circumscribes the Poincaré map, P is a partition of the interval I, N is the number of $\Re^2$ intervals of the partition P, and N_0 is the number of intervals of the partition P that do not contain a pair $(\hat{\xi}_3(t^*), d\hat{\xi}_3/d\hat{t}(t^*))$.

Figure 8(a) shows Poincaré maps for different flight speeds, while Figure 8(b) shows the *DIRA* parameter of these Poincaré maps as a function of the flight speed (KTAS). The *DIRA* parameter allows to determine the flight speed range with high level of chaos, giving so a better understanding of the chaotic motion of the system.

7 Conclusions

This paper analyses the effect of *freeplay/hysteresis* local structural nonlinearities on the aeroelastic behaviour of a missile configuration. The first part is devoted to review the Airworthiness Regulations and methods/tools that are currently used for preventing and/or predicting the effect of structural nonlinearities from the aeroelastic standpoint. Among all methods, this paper uses the *time-domain integration* of the aeroelastic equations written into the state-space form.

The time-domain integration needs of specific

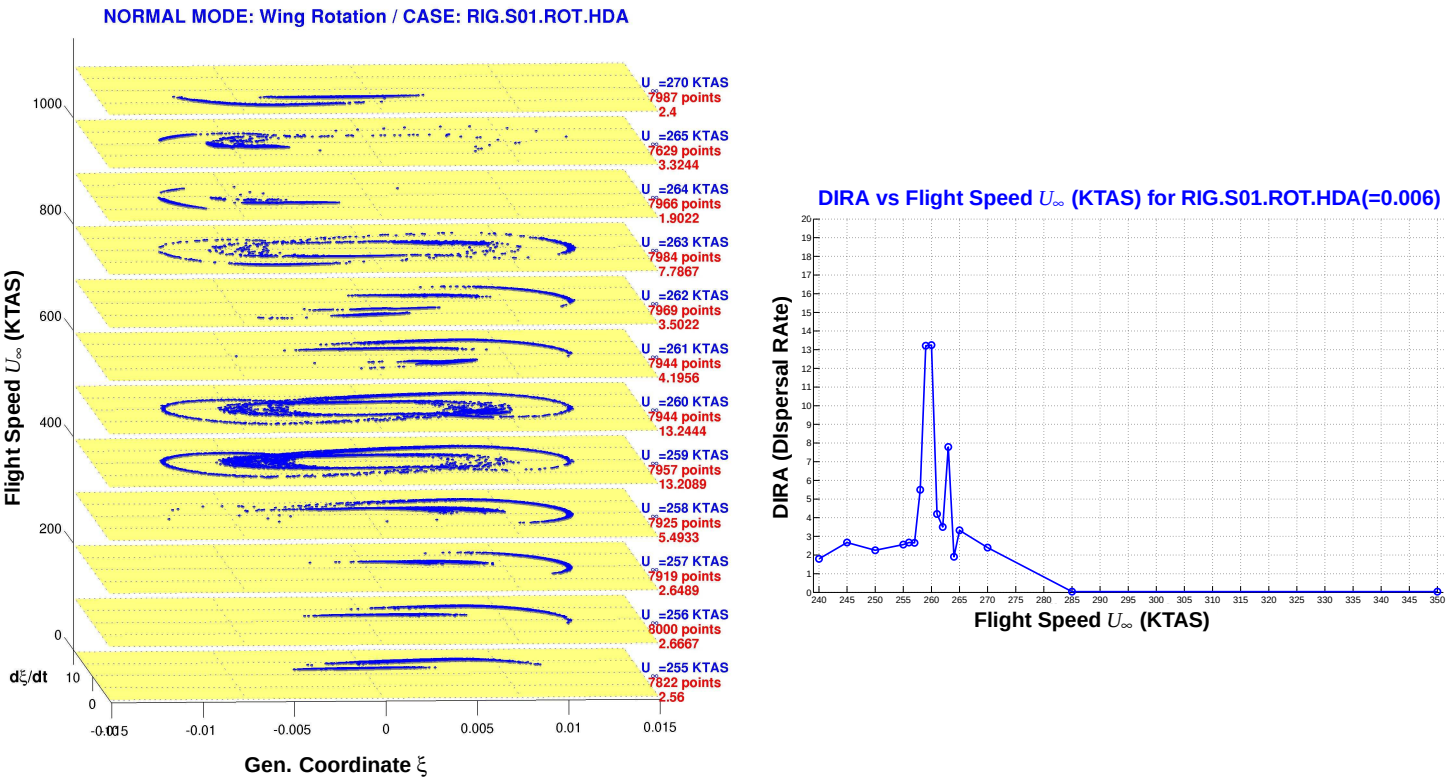

Fig. 8 Left figure: Poincaré maps for different flight speeds. Right figure: DIRA parameter vs flight speed.

tools that are detailed into the second part of the paper. The freeplay/hysteresis nonlinearities are piecewise linear functions that modify the stiffness properties as the system switches into the different zones. This means that the system changes its normal modes but, for avoiding discontinuities at the corner points, an unique normal modes base is needed. This paper uses the IOB modal base, that is built by completing the nominal normal modes base (nominal stiffness) with the rigid body mode that appears when the stiffness of the nonlinear DOF is dropped to zero (system inside the freeplay deadband zone). In addition, it is necessary a *corner capturing module* for switching the state-space equations at the exact corner point. This paper uses the *illinois method*, a variation of the well-known *regula-falsi method*.

Additional modules are useful when dealing with time-domain integration: real-time response detectors, PSD analyses, and chaotic motion detectors. This paper introduces the *Dispersal Rate DIRA* parameter for quantifying the chaos intensity.

All this methodology and tools have been applied to a missile-type configuration with a freeplay/hysteresis nonlinearity in different DoFs (lateral, yaw, and control surface rotation). Results show that nonlinearities clearly modify the classical aeroelastic behaviour, changing the linear flutter speed and introducing LCOs and chaotic motion below the nonlinear flutter speed. The missile configuration has served as a test case for validating the methodology, procedures, and tools detailed into the paper. UPM and Airbus Military are working on extending the results to aircraft-type complex configurations with nonlinearities at control surfaces.

References

[1] E. Albano and W.P. Rodden. A doublet-lattice method for calculating lift distribution on oscillating surfaces in subsonic flow. *AIAA Journal*, 7(2):279–285, 1969.

[2] H. Alighanbari and S.M. Hashemi. Bifurcation analysis of an airfoil containing a cubic structural nonlinearity and subjected to two-dimensional incompressible flow. *43rd*

AIAA/ASME/ASCE/AHS/ASC Structures, Structural Dynamics, and Materials Conference. AIAA 2002-1206., pages 1146–1153, 2002.

[3] F. Arévalo. Dynamic analysis by numerical integration: Newmark's time-integration method. Technical report, AIRBUS MILITARY Technical Note NT-T-AA0-03003, 2003.

[4] F. Arévalo. Aeroelasticidad de una aeronave en presencia de nolinealidades estructurales concentradas. Phd thesis, Escuela Técnica Superior de Ingenieros Aeronáuticos ETSIA, Universidad politécnica de Madrid UPM, 2008. Presented for PhD degree at ETSIA.

[5] J.J. Block and T.W. Strganac. Applied active control for a nonlinear aeroelastic structure. *Journal of Guidance, Control, and Dynamics*, 21(6):838–845, 1998.

[6] O. Brase and W. Eversman. Application of transient aerodynamics to the structural nonlinear problem. *Journal of Aircraft*, 25(11):1060–1068, 1988.

[7] T.H. Burkhart. Subsonic transient lifting surface aerodynamics. *Journal of Aircraft*, 14(1):44–50, 1977.

[8] W.H. Cheng and W.B. Lin. Nonlinear flutter of loaded lifting surfaces (i) and (ii). *Journal of the Chinese Society of Mechanical Engineers*, 14(5):446–466, 1993.

[9] K.W. Chung, C.L. Chan, and B.H.K. Lee. Bifurcation analysis of a 2d aeroelastic system with freeplay structural nonlinearity by a perturbation-incremental method. *Journal of Sound and Vibration*, 299, 2007.

[10] D. Eller. On an efficient method for time-domain computational aeroelasticity. *Technical Report TRITA/AVE 2006:1, AVE, Kungliga Tekniska Högskolan, Stockholm, PhD Thesis*, 2006.

[11] D. Eller. Friction, freeplay and flutter of manually controlled aircraft. *IFASD 2007*, pages 581–595, 2007.

[12] Y.C. Fung. *An introduction to the theory of aeroelasticity*. Dover Publications Inc., 1993.

[13] P. Gold and M. Karpel. Reduced-size aeroservoelastic modeling and lco simulations with structurally nonlinear actuators. *Journal of Aircraft*, 45(2), 2008.

[14] M. Karpel. Design for active flutter suppression and gust alleviation using state-space aeroelastic modeling. *Journal of Aircraft*, 19(3):221–227, 1982.

[15] J. Ko, T.W. Strganac, and A.J. Kurdila. Adaptive feedback linearization of the control of a typical wing section with structural nonlinearities. *Nonlinear Dynamics*, 18(3):289–301, 1999.

[16] G. Kuruvila, R.E. Bartels, M.S. Hong, and K.G. Bhatia. Nonlinear aeroelastic analysis using a time-accurate navier-stokes equations solver. *International Forum of Aeroelasticity and Structural Dynamics IFASD*, 2007.

[17] B.H.K. Lee and P. LeBlanc. Flutter analysis of a two-dimensional airfoil with cubic nonlinear restoring force. Phd thesis, National Aeronautical Establishment, Aeronautical Note 36, National Research Council (Canada), 1986.

[18] R. Vepa. On the use of padé approximants to represent unsteady aerodynamic loads for arbitrarily small motions of wings. *AIAA Paper 76-17*, 1976.

[19] G.A. Vio and J.E. Cooper. Limit cycle oscillations prediction for aeroelastic systems with discrete bilinear stiffness. *Journal of Applied Math. and Mech.*, 3:110–119, 2005.

7.1 Copyright Statement